International Journal of Mechanical, Industrial and Aerospace Sciences
ISSN: 2517-9950
Vol:6, No:2, 2012

3D Sensing and Mapping for a Tracked Mobile Robot with a Movable Laser Ranger Finder

Toyomi Fujita

***Abstract*—**This paper presents a sensing system for 3D sensing and mapping by a tracked mobile robot with an arm-type sensor movable unit and a laser range finder (LRF). The arm-type sensor movable unit is mounted on the robot and the LRF is installed at the end of the unit. This system enables the sensor to change position and orientation so that it avoids occlusions according to terrain by this mechanism. This sensing system is also able to change the height of the LRF by keeping its orientation flat for efficient sensing. In this kind of mapping, it may be difficult for moving robot to apply mapping algorithms such as the iterative closest point (ICP) because sets of the 2D data at each sensor height may be distant in a common surface. In order for this kind of mapping, the authors therefore applied interpolation to generate plausible model data for ICP. The results of several experiments provided validity of these kinds of sensing and mapping in this sensing system.

***Keywords*—**Laser Range Finder, Arm-Type Sensor Movable Unit, Tracked Mobile Robot, 3D Mapping.

I. Introduction

A 3D sensing is a very important function for a mobile robot to get precise surrounding information as possible to move working field efficiently. A 2D laser range finder (LRF) is widely used for a 3D sensing because it can detect wide area fast and can obtain 3D information easily.

In order to expand the 2D LRF to 3D sensing, the authors have proposed a LRF sensing system, as shown in Fig. 1, that has an arm-type sensor movable unit which is mounted on a tracked mobile robot [1]. This sensing system can change position and orientation of the sensor in a movable area of the arm unit and face it at a right angle according to a variety of shape. The robot is therefore able to avoid occlusion in the sensing of complex terrain such as valley, deep hole, inside the gap, and so on.

In addition, this sensing system is able to change the height of the LRF by keeping its orientation flat for efficient sensing. In this way, the height of LRF can be changed at equal interval by lifting it up and down vertically by the arm-type sensor movable unit. 3D map can be obtained by combining 2D maps in individual heights of the LRF. This sensing can avoid a problem on accumulation point in conventional 3D sensing method by a LRF with a rotating mechanism.

If a robot is moving in this mapping, however, it may be difficult to apply mapping algorithms such as the iterative closest point (ICP) because sets of the 2D data at each sensing height in a common surface may be too distant and scattered to get corresponding points.

T. Fujita is with Tohoku Institute of Technology, 35-1 Yagiyama Kasumi-cho, Taihaku-ku, Sendai 982-8577, Japan (phone: +81-22-305-3228; fax: +81-22-305-3202; e-mail: t-fujita@tohtech.ac.jp).

We consider applying interpolation in order to solve this problem and generate plausible model data for ICP. This paper presents the 3D mapping method as well as advantages of this sensing system that uses a LRF equipped with an arm-type movable unit. Section II describes related work. Section III introduces an overview of the developed tracked mobile robot and sensing system. Section IV presents possible sensing modes by this system and explains the sensing abilities and advantages. Section V describes fundamental experiments which were employed to confirm 3D sensing ability of this system. Section VI explains the method for 3D mapping using interpolation and shows experimental result.

II. Related Work

A. 3D Sensing using LRF

A 2D laser range finder (LRF) is widely used for a 3D sensing because it can detect wide area fast and can obtain 3D information easily. A lot of 3D sensing systems using the LRF have been presented in earlier studies [2]–[4]. In those measurement systems, multiple LRF sensors are installed in different directions [5], or a LRF is mounted on a rotatable unit [6], [7]. It is however still difficult for those systems to do sensing more complex terrain such as valley, deep hole, or inside the gap due to occlusions. As the other related work, for example, [8] proposed the combination of 2D LRF and stereo vision for 3D sensing. This method however increases the cost of sensing system.

Another study [9] has showed a similar sensing system in which a range imager has been used to construct a terrain model of stepfields. The range imager in the system however was fixed at the end of a pole in this system. Our proposed system is more flexible because the sensor can be actuated.

B. 3D Mapping

A lot of works have considered the method for 3D map building by 2D laser scanners. One of famous methods is to use the iterative closest point (ICP) algorithm [10]. Nuchter et al. presented 3D mapping using the ICP [6] and 6D simultaneous localization and mapping (SLAM) [11]. Thrun et al. proposed probabilistic terrain analysis algorithm for high speed terrain classification [12]. Nagatani et al. proposed a mapping method based on the ICP algorithm and the normal distribution transform (NDT) algorithm [13].

In this study, we try to use the conventional ICP method to obtain 2D map on each height of the LRF in presented sensing system. In order to apply ICP, the sensing points must intersect at a common surface. If the robot is moving, however, it is difficult to make intersected points at a common surface because

the sensor position is also moving at different heights. This study uses interpolation to make the intersected points for the robot that is running. The method is inspired by the work by Kehagias et al. in which interpolation is used in order to improve the performance of SLAM algorithms [14].

III. System Overview

This section describes the tracked mobile robot and sensing system which have been designed and developed in this study.

A. Tracked Robot

We have developed a tracked mobile robot toward rescue activities. Fig. 1 shows an overview of the robot system. The robot has two crawlers at the both sides. A crawler consists of rubber blocks, a chain, and three sprocket wheels. The rubber blocks are fixed on each attachment hole of the chain. One of the sprocket wheels is actuated by a DC motor to drive a crawler for each side. The size of the robot is 400 mm (length) × 330 mm (width) × 230 mm (height), when the sensor is descended on the upper surface of the robot.

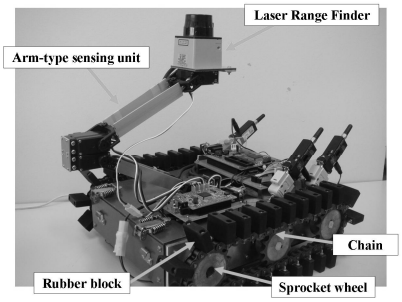

Fig. 1 Developed tracked mobile robot and sensing system

B. Arm-type Sensor Movable Unit

The arm-type sensor movable unit consists of two links having a length of 160 mm and has three degrees of freedom. The links are connected by two RC servo motors as a joint in order to make the sensor flat easily when folded. Another two joints are also attached to the both ends of the connecting links; one is connected to the sensor at the end and the other is mounted on the upper surface of the robot. The robot can lift the sensor up to the height of 340 mm and change its position and orientation by rotating those joints.

C. Sensors

HOKUYO URG-04LX [15] is used as the LRF sensor in this system. This sensor can scan 240 degrees area and obtain distance data every 0.36 degree on a 2D plane. This sensor equipped at the end of the arm-type unit is able to change its position and orientation.

We have also installed an acceleration sensor around three orthogonal axes to detect tilt angle of the robot body and to control the orientation of the LRF to be flat corresponding to the tilt angle. The use of this sensor enables the arm-type movable unit to change the height of the LRF with keeping its orientation.

D. Control System

The control system of this robot system consists of two embedded micro computers: Renesas SH-2/7045F and H8/3052F for controlling the main robot and the arm-type sensor movable unit respectively. A Windows/XP host PC manages all controls of those units as well as scanned data of the sensor. The host PC sends movement commands to individual embedded micro computers for the robot and arm-type unit and request for sensor data acquisition to the sensor. The sensor can commu- nicate directly with the host PC. All communications for those protocols are made by wireless serial communications using bluetooth-serial adapters: SENA Parani-SD100.

E. Calculation of 3D Sensing Position

In this system, the robot can obtain 3D sensing positions from the sensor data of the LRF and the orientation of the robot obtained by the acceleration sensor. When $\boldsymbol{p}_s$ shows a position vector of sensed point by the sensor, the 3D sensing position vector $\boldsymbol{p}$ in the base coordinate system can be calculated by

$$\begin{pmatrix} \boldsymbol{p} \\ 1 \end{pmatrix} = {}^0\boldsymbol{H}_r \, {}^r\boldsymbol{H}_s \begin{pmatrix} \boldsymbol{p}_s \\ 1 \end{pmatrix} \quad (1)$$

where ${}^0\boldsymbol{H}_r$ shows a homogeneous matrix that represents a transformation between the base position and the robot body, and ${}^r\boldsymbol{H}_s$ shows a homogeneous matrix that represents a transformation between the robot body and the sensor.

IV. Sensings by Arm-type Sensor Movable Unit

The mechanism of this sensing system enables the LRF to change position and orientation to face at a right angle corresponding to a variety of shape. For example, this sensing system is able to do sensing deep bottom area without occlusions as shown in Fig. 2. Because the occlusion can be avoided by this mechanism even for complex terrain, the robot can measure a 3D shape such as valley, gap, upward or downward stairs more accurately than conventional 3D sensing system with the rotatable LRF. In addition, a robot can do sensing more safely by this method because the robot does not have to stand at close to the side of border. It is important when the robot needs to work in an unknown site such as disaster area.On the other hand, this arm-type movable unit can change the height of the LRF by keeping its orientation flat. In this way, 2D shape information in a horizontal plane is detected in each height with even interval. Consequently, the 3D shape of surrounding terrain can be obtained more efficiently by moving the LRF up vertically and keeping its orientation flat. Detecting tilt angle of the robot by the acceleration sensor installed in the robot body, the robot can performs this kind of sensing even when it is on rough surface.

V. 3D Shape Sensing

We employed fundamental experiments to confirm basic sensing ability of the sensing system. In the experiments, several kinds of shape – upward stairs, a valley and a cave under the robot – were measured by the sensing method presented in the previous section.

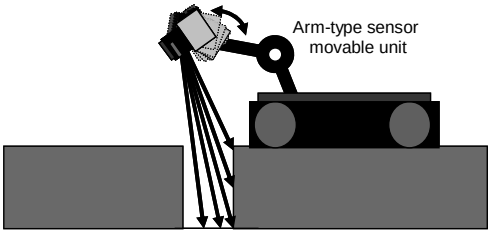

Fig. 2 Sensing of deep bottom area without occlusions

A. Upward Stairs

Fig. 3 shows an overview of the experimental environment for a measurement of upward stairs. The stairs are located 1100 mm ahead of the robot. Each stair is 80 mm in height and depth. The robot stayed at one position and the LRF sensor was lifted vertically by the arm-type unit from the upper surface of robot to the height of 340 mm with equal interval of 50 mm. Each scanning of the sensor was performed for each height. The robot was tilted 10 degrees to confirm the usefulness of the acceleration sensor in the robot. The robot detected its orientation by the sensor and controlled the height of the LRF according to the orientation.

Fig. 4 shows the measurement result; almost same shape to actual environment was obtained in this sensing system.

Fig. 3 Overview of measurement for upward stairs

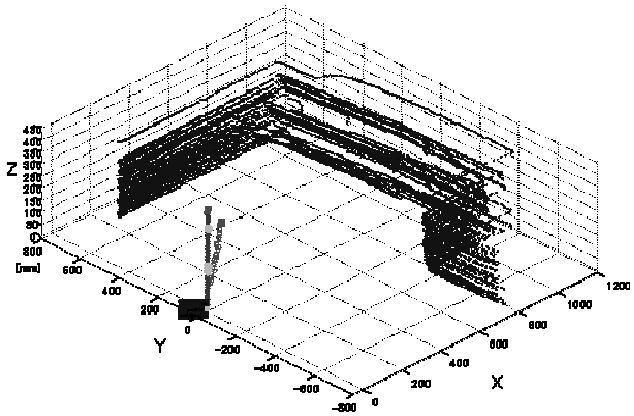

Fig. 4 Measured 3D terrain of upward stairs

B. Valley

A shape of a valley was set up as an experimental environment. Fig. 5 shows its schematic diagram. The valley was 610 mm deep and 320 mm long. We gave reference points at each corner of the shape to estimate actual error value on measurement points. Actual position values of these points are described in the figure.

The robot stayed at one position, 250 mm away from the border, and the sensor was located over the valley by the arm-unit. The sensor angle only was changed and the other joint angles of the arm were kept to fix sensor position, as the same way illustrated in Fig. 2. The rotation angle of the LRF varied from 0 degree to 90 degrees every 1.8 degrees. Each scanning was performed for each sensor angle.

Fig. 6 shows the measurement result. We can see very similar shape to the actual valley. The measurement positions for reference points are also denoted in the figure. The position values show that accurate position can be sensed by this sensing system. Table I shows actual and measured distance with error ratio values on the reference points. Even though the error ratio for the point e was higher, the most of points had the value less than about 5 %.

C. Cave under Robot

We employed an experiment of measurement for a shape of a cave under the robot. Fig. 7 shows a schematic diagram of the environment in the experiment. The dimension of the cave was set to 880 mm (width) × 400 mm (height) × 600 mm (depth). Eight reference points were given at each corner of the cave to estimate actual errors.

The robot stayed at one position as previous experiments and the sensor was located in front of the cave by the arm-unit. Each of joints except for the last joint was rotated to fixed angle to keep the sensor position. The angle of the LRF only varied from 0 degree to 70 degrees every 1.8 degrees. Each scanning was performed for each sensor angle.

Fig. 8 shows the measurement result. This result also showed almost the same shape to the actual environment. The measurement position values for reference points are also denoted in the figure. Table II shows actual and measured distance with error ratio values on the eight reference points. The error ratios demonstrated accurate sensing in this system; the maximum was 4.4 % and average was 1.9 % for all points.

VI. 3D Mapping

A. Mapping using ICP

Specially this study considers the situation in which robot runs in the environment with moving LRF up and down vertically. In this case robot can obtain surrounding 2D planar shapes of the terrain from the LRF. The arm-type sensor movable unit of this sensing system can do it easily. We can build map with localization using SLAM techniques, such as ICP, presented in a lot of earlier studies. In this case, however, we need to consider that the height of LRF may be different in each scanning. Basically, two sets of scanned data by LRF have to be on the same plane: the same height in this case. We need to get two sets of data on the same height to get corresponding points. However, in most of cases, it may not be assured that the sensing is done at the same height of LRF.

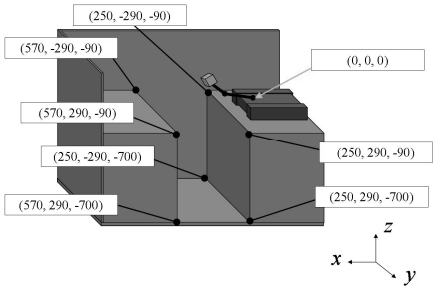

Fig. 5 Experimental environment with reference points for a shape of a valley (unit: mm)

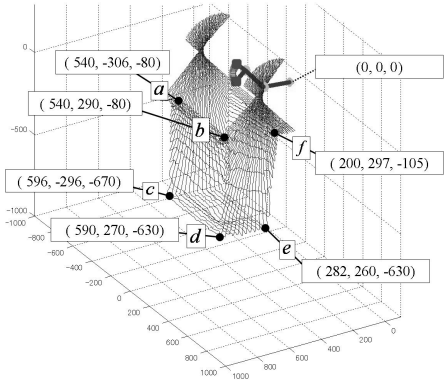

Fig. 6 Measured shape of a valley with measurement position values for reference points

TABLE I
MEASUREMENT DISTANCES AND ERROR RATIOS ON REFERENCE POINTS FOR THE SHAPE OF A VALLEY

	distance mm			
point	actual	measured	error	error ratio [%]
a	645.8	625.8	20.0	3.1
b	645.8	618.1	27.7	4.3
c	948.2	944.3	3.8	0.4
d	948.2	904.4	43.8	4.6
e	797.9	737.6	60.3	7.6
f	393.3	373.1	20.2	5.1

B. Interpolation of Scan Data

In order to solve this problem, we apply interpolation to generate plausible model data for ICP. Fig. 9 shows the concept. Suppose that the robot is moving from right to left and three sensings have been made in sequence. In the third sensing, the sensing height is between the first and second heights. It is generally impossible to apply ICP algorithm among three sets of sensing point data because there are no corresponding data which should be a reference model of the map. In order to generate the reference model, an interpolation is applied between the first and second data for the height of the third sensing. The black triangles in Fig. 9 indicate the interpolated points for the reference model. These points are used as the corresponding points to do ICP.

The interpolation is applied to the sensor position and orientation for simplicity; it consists of a linear interpolation for the position vector and a spherical linear interpolation for the rotation [16].

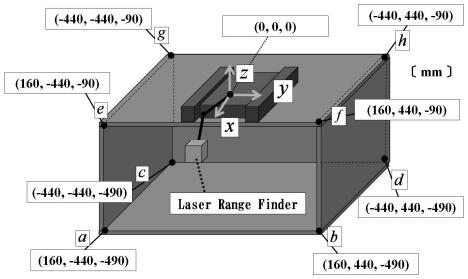

Fig. 7 Experimental environment for a shape of a cave under the robot with reference points

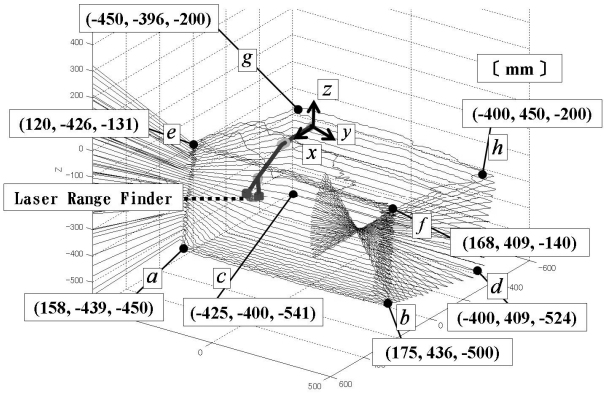

Fig. 8 Measured shape of a cave under the robot with measurement position values for reference points (unit: mm)

TABLE II
MEASUREMENT DISTANCES AND ERROR RATIOS ON REFERENCE POINTS FOR THE SHAPE OF CAVE UNDER THE ROBOT

	distance mm			
point	actual	measured	error	error ratio [%]
a	677.7	648.2	29.5	4.4
b	677.7	686.1	8.4	1.2
c	792.0	795.8	3.8	0.5
d	792.0	775.8	16.2	2.0
e	476.8	461.6	15.2	3.2
f	476.8	463.8	13.0	2.7
g	628.7	631.9	3.2	0.5
h	628.7	634.4	5.7	0.9

The linear interpolation for the position vector $\boldsymbol{t_i}$ from two vectors $\boldsymbol{t_1}$ and $\boldsymbol{t_2}$ is represented by

$$t_i = (1-r)\, t_1 + r t_2 \tag{2}$$

where r is the ratio of interpolation. In this study the ratio of the height of the sensor was given for r so that

$$r = \frac{h_i - h_1}{h_2 - h_1} \tag{3}$$

where $\boldsymbol{h_i}$ is the current height of the sensor, h_1 and h_2 are the heights in previous sensings ($h_2 > h_i > h_1$). $\boldsymbol{t_i}$, $\boldsymbol{t_1}$, and $\boldsymbol{t_2}$ are obviously corresponding to h_i, h_1, and h_2 respectively.

In order for the spherical linear interpolation, the rotation is represented by quaternion $Q = (q_0, \boldsymbol{q})$. Assuming $\boldsymbol{v}$ is the

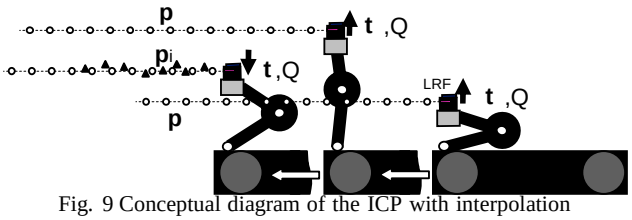

Fig. 9 Conceptual diagram of the ICP with interpolation

vector of the rotational axis and θ is the rotational angle around the axis, the vector $\boldsymbol{q} = (q_1, q_2, q_3)^{\mathrm{T}}$ is defined as

$$\boldsymbol{q} = \sin\left(\frac{\theta}{2}\right)\boldsymbol{v} \tag{4}$$

and the q_0 is given by

$$q_0 = \cos\left(\frac{\theta}{2}\right). \tag{5}$$

The spherical linear interpolation of the quaternion, Q_i, from Q_1 and Q_2, which are corresponding to the rotations of the sensor at height h_1 and h_2, is given by

$$Q_i = Q_1 \frac{\sin((1-r)\omega)}{\sin\omega} + Q_2 \frac{\sin(r\omega)}{\sin\omega} \tag{6}$$

where

$$\omega = \cos^{-1}(Q_1 \cdot Q_2). \tag{7}$$

$(Q_1 \cdot Q_2)$ represents an inner product of quaternion Q_1 and Q_2 .

From this computation of the interpolation, we can obtain a homogeneous matrix $\boldsymbol{H}_{i1}$ and $\boldsymbol{H}_{i2}$ to compute interpolation data $\boldsymbol{p}_i$ from two sets of scan data $\boldsymbol{p}_1$ and $\boldsymbol{p}_2$ respectively. In this study the interpolation of scan data $\boldsymbol{p}_i$ are determined by

$$\begin{pmatrix}\boldsymbol{p}_i\\1\end{pmatrix} = \begin{cases}\boldsymbol{H}_{i1}\begin{pmatrix}\boldsymbol{p}_1\\1\end{pmatrix} & (r \le 0.5),\\ \boldsymbol{H}_{i2}\begin{pmatrix}\boldsymbol{p}_2\\1\end{pmatrix} & (r > 0.5).\end{cases} \tag{8}$$

C. Experiment

A basic experiment of 3D mapping by this method was employed. In the experiment, robot moved forward in a flat corridor as shown in Fig. 10, which is the upper view, with moving the LRF up and down and made each planar sensing for every 40 cm distance. Fig. 11 shows an overview of the experiment. The LRF was moved vertically from the upper surface of the robot body to the height of 340 mm.For the purpose of validation of proposed method, the sensing positions were intentionally scattered. ICP data at the sensing locations were combined using odometry information of the robot.

Fig. 12 shows the built map in this experiment. The built data for each sensing height were described by individual different line. The robot position in each sensing is indicated by a circle and the sensor height at the position is indicated by a square. This result shows valid 3D shapes of the environment. Obstacles against the wall were also detected at the almost correct position in the result.

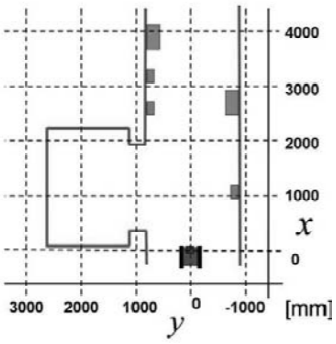

Fig. 10 Experimental environment for 3D mapping (upper view)


Fig. 11 Overview of 3D mapping experiment

VII. Discussion

This study has employed fundamental experiments for 3D shape sensing for upward stairs, a valley, and a cave under the robot. From Fig. 4, Fig. 6, and Fig. 8, we can see that the almost same shape was measured respectively. These results therefore confirm that this system is useful for shape sensing in complex environment.The result of 3D sensing of a valley, shown in Fig. 6, especially indicates an advantage of the presented sensing system; it enables to do sensing deep bottom area without occulusions. In addition, the robot can do it safely because it does not have to stand at close to the border. The reason why the error ratio of 7.6% occurred for the reference point e, as shown in Table I, is that the position was acute angle for the sensor. This error could be improved if the location of the sensor so that it can face to the right position to the point.The result of 3D measurement for a cave under the robot also demonstrated another ability and strong advantage of the sensing system. Fig. 8 showed that this system enables us to obtain 3D information for such a shape which any conventional sensing system has never been able to measure. Moreover, the error ratios showed accurate sensing as shown in Table II. This sensing system must be useful for 3D shape sensing specially in rough or rubble environments such as disaster area.The experimental result described in Section VI indicated that presented method for 3D mapping by this sensing system is useful. Fig. 12 shows almost actual shapes and positions of environment including obstacles.

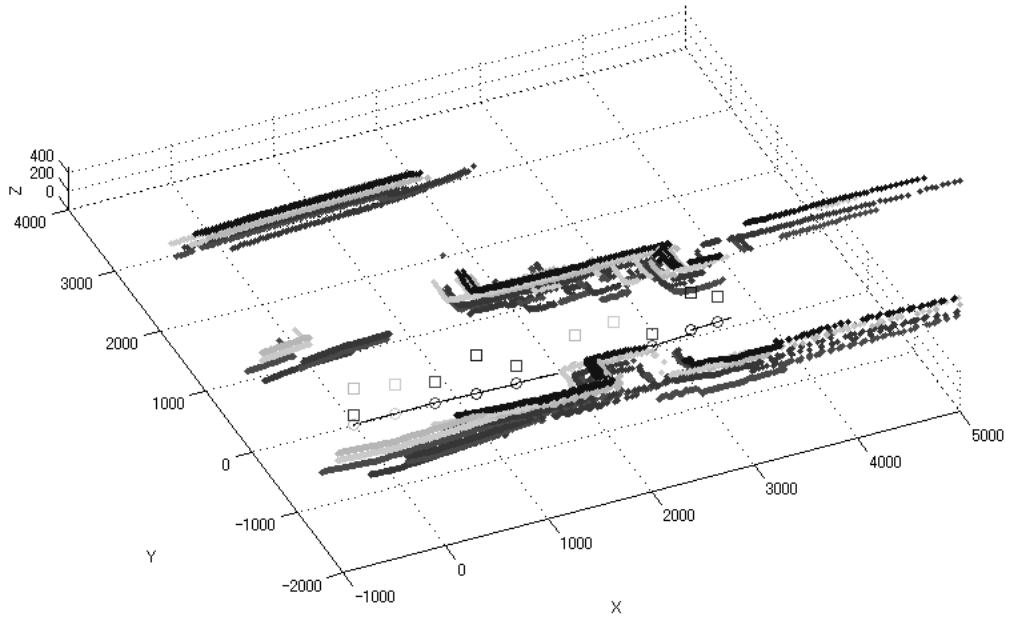

Fig. 12 Experimental result of 3D mapping

The result of the experiment suggests that the interpolation is useful for 3D mapping when robot is moving fast. Some errors however occurred in some corners. These errors may come from some odometry errors due to slip of tracks in the movement as well as the error in ICP operation with incorrect data by interpolation. More robust mapping by corresponding vertical sensing points should be considered.

VIII. Conclusion

This paper presented a 3D sensing system with arm-type sensor movable unit and 3D mapping method using interpolation for the ICP algorithm. The experimental results showed that this system is useful for accurate and safe 3D shape sensing as well as 3D mapping. Because this sensing system has a variety of sensing mode, we need further consideration of the sensing and mapping strategies for more complex environment.

References

[1] Toyomi Fujita and Yuya Kondo, "3D Terrain Measurement System with Movable Laser Range Finder", Proceedings of 2009 IEEE International Workshop on Safety, Security, and Rescue Robotics (SSRR 2009), 2009.

[2] M. Hashimoto, Y. Matsui, and K. Takahashi, "Moving-object tracking with in-vehicle multi-laser range sensors," Journal of Robotics and Mechatronics, vol. 20, no. 3, pp. 367–377, 2008.

[3] T. Ueda, H. Kawata, T. Tomizawa, A. Ohya, and S. Yuta, "Mobile SOKUIKI Sensor System-Accurate Range Data Mapping System with Sensor Motion," in Proceedings of the 2006 International Conference on Autonomous Robots and Agents.

[4] K. Ohno and S. Tadokoro, "Dense 3D map building based on LRF data and color image fusion," in 2005 IEEE/RSJ International Conference on Intelligent Robots and Systems, 2005.(IROS 2005), 2005, pp. 2792–2797.

[5] J. Poppinga, A. Birk, and K. Pathak, "Hough based terrain classification for realtime detection of drivable ground," Journal of Field Robotics, vol. 25, no. (1-2), pp. 67–88, 2008.

[6] A. Nuchter, K. Lingemann, and J. Hertzberg, "Mapping of rescue environments with kurt3d," in In Proc. IEEE SSRR 2005, 2005, pp. 158–163.

[7] Z. Nemoto, H. Takemura, and H. Mizoguchi, "Development of Small-sized Omni-directional Laser Range Scanner and Its Application to 3D Background Difference," in Industrial Electronics Society, 2007. IECON 2007. 33rd Annual Conference of the IEEE, 2007, pp. 2284–2289.

[8] L. Iocchi, S. Pellegrini, and G. Tipaldi, "Building multi-level planar maps integrating LRF, stereo vision and IMU sensors," in Safety, Security and Rescue Robotics, 2007. SSRR 2007. IEEE International Workshop on, 2007, pp. 1–6.

[9] R. Sheh, M. Kadous, C. Sammut, and B. Hengst: "Extracting terrain features from range images for autonomous random stepfield traversal," in Safety, Security and Rescue Robotics, 2007. SSRR 2007. IEEE International Workshop on, 2007, pp. 1–6.

[10] P. J. Besl and N. D. Mckay: A method for registration of 3-d shapes, IEEE Transactions on Pattern Analysis and Machine Intelligence, 14(2), 239–256, August 2002.

[11] Nuchter, A., Lingemann, K., Hertzberg, J. and Surmann, H., "6D SLAM–3D mapping outdoor environments," Journal of Field Robotics, vol. 24, issue 8-9, pp.699-722, 2007.

[12] S. Thrun, M. Montemerlo, and A. Aron, "Probabilistic terrain analysis for high-speed desert driving," in Proceedings of Robotics Science and Systems Conference, 2006.

[13] Nagatani, K., Matsuzawa, T., Yoshida, K., "Scan-point planning and 3-d map building for a 3-d laser range scanner in an outdoor environment", Springer Tracts in Advanced Robotics, vol. 62, pp. 207-217, 2010.

[14] A. Kehagias, J. Djugash, and S. Singh,"Range-only SLAM with Interpolated Range Data," tech. report CMU-RI-TR-06-26, Robotics Institute, Carnegie Mellon University, 2006.

[15] Hokuyo Automatic Co., Ltd.: in http://www.hokuyo-aut.co.jp.

[16] T. Barrera , A. Hast and E. Bengtsson "Incremental spherical linear interpolation", Proc. SIGRAD, vol. 13, pp. 7 2004.